ACCSCIENCE PUBLISHING

Innovative Medicines & Omics

ORIGINAL RESEARCH ARTICLE

Antibacterial emulsion based on methyl cellulose and lavender essential oil: Rheology and drug release kinetics

Gözde Bayer[1], Amirreza Shayganpour[2], and Ilker S. Bayer[3]*

[1]Gempa Electromechanical Engineering Ltd. Co., Çankaya, Ankara, Türkiye

[2]Smart Materials, Italian Institute of Technology, Genova, Liguria, Italy

[3]I2Pure Corporation, Ashburn, Virginia, United States of America

Abstract

Topical antibacterial emulsions require optimized formulation strategies to maximize drug release, bioavailability, and antimicrobial efficacy while maintaining desirable rheological properties. This study presents the formulation and characterization of an antibacterial emulsion comprising methyl cellulose, triacetin, triethyl citrate, and a synergistic blend of benzyl alcohol, phenylethanol, and lavender essential oil, designed for topical drug delivery. Emulsions were prepared by shear mixing and ultrasonic processing and evaluated for rheological behavior, essential oil release kinetics, and antimicrobial efficacy. Mechanical mixing physically disrupts macromolecular matrix entanglements, accelerating the dispersion of essential oils and significantly enhancing active terpene bioavailability, thereby driving rapid bactericidal kinetics. Viscoelastic and shear-thinning properties were modeled using Maxwell, Cross, and Herschel–Bulkley frameworks incorporating thixotropic considerations, revealing a yield stress of 8 Pa and strong structural recovery behavior. Ultraviolet–Visible spectrophotometry-based drug release studies demonstrated that shear mixing significantly enhanced essential oil release rates, with the Weibull model providing the best fit to the release profiles. Antibacterial testing against *Escherichia coli* and ten genetically diverse strains of lactic acid bacteria showed that aromatic alcohol-containing formulations significantly reduced minimum inhibitory concentration and minimum bactericidal concentration values, confirming synergistic antibacterial action. Optical density monitoring and bacterial viability modeling revealed substantially improved bactericidal activity under mixing conditions, attributed to enhanced dispersion and bioavailability of the essential oil. These results demonstrate that the formulation method plays a decisive role in both physical and antimicrobial performance, supporting the potential of these emulsions for treating skin infections and limiting the spread of antibiotic-resistant bacteria.

Keywords: Antibacterial; Emulsion; Essential oil; Methyl cellulose; Drug release; Viscoelasticity

***Corresponding author:**
Ilker S. Bayer
(ilker@i2pure.com)

Citation: Bayer G, Shayganpour A, Bayer IS. Antibacterial emulsion based on methyl cellulose and lavender essential oil: Rheology and drug release kinetics. *Innov Med Omics*. 2026;3(4):026220029. doi: 10.36922/IMO026220029

Received: May 27, 2026

Revised: June 20, 2026

Accepted: June 22, 2026

Published online: July 30, 2026

Copyright: © 2026 Author(s). This is an Open-Access article distributed under the terms of the Creative Commons Attribution License, permitting distribution, and reproduction in any medium, provided the original work is properly cited.

Publisher's Note: AccScience Publishing remains neutral with regard to jurisdictional claims in published maps and institutional affiliations.

1. Introduction

Topical emulsions represent a cornerstone of dermatological and transdermal drug delivery, offering a versatile semisolid platform capable of incorporating both hydrophilic and lipophilic active agents within oil-water systems stabilized by surfactants or polymers.[1,2] Their widespread clinical adoption stems from favorable attributes, including ease of application, good skin adhesion, spreadability, and the capacity to maintain prolonged contact with the target tissue. Recent innovations in formulation science have enabled the integration of advanced nanocarriers such as nanoemulsions, solid lipid nanoparticles, and liposomes, significantly improving drug encapsulation efficiency, physicochemical stability, and skin permeability.[1–3] These advances have been further supported by progress in manufacturing technologies, including high-pressure homogenization, ultrasonic emulsification, and low-energy self-assembly methods, which afford finer control over droplet size distribution, interfacial architecture, and formulation rheology.[4,5]

The skin, while an accessible delivery site, presents a formidable barrier to drug transport, primarily through the densely packed lipid lamellae of the stratum corneum. Overcoming this barrier is a central challenge in the design of topical emulsions, addressed through the incorporation of penetration enhancers, micro- and nanoencapsulation strategies, and rheologically tuned bases that promote prolonged skin contact and controlled drug flux.[6,7] Lipid-based and nanoemulsion vehicles enable drugs to partition into deeper skin layers or enter systemic circulation while maintaining controlled release characteristics, making them attractive for both local and transdermal therapeutic applications.[8,9] Beyond passive diffusion, emerging smart delivery platforms responsive to physiological stimuli such as temperature, pH, or enzymatic activity are being developed to enable site-specific, on-demand drug release with reduced systemic side effects.[10] Complementary advances in three-dimensional skin modeling and non-invasive imaging have improved *in vitro–in vivo* correlation, accelerating the rational development of semisolid transdermal therapeutics.[11] Collectively, these innovations are broadening the therapeutic scope of topical emulsions beyond dermatology into systemic drug administration, hormonal therapy, and pain management.

Drug release from topical emulsions is governed by a complex interplay of physicochemical mechanisms, including diffusion, partitioning, matrix erosion, and swelling.[11–13] Diffusion-controlled release remains the most prevalent, driven by concentration gradients between the emulsion matrix and the stratum corneum, while the oil-water partition coefficient of the active agent determines the efficiency of its transfer into skin tissue. In polymer-rich or hydrophilic emulsion systems, swelling- and erosion-dominated release may become significant, particularly under the moisture-rich conditions of occluded skin.[14] Mathematical models, including the Higuchi, Korsmeyer–Peppas, first-order, and Weibull frameworks, are routinely employed to characterize and predict these release mechanisms, providing mechanistic insight that guides formulation optimization.[12,14] Nanoencapsulation approaches, such as solid lipid nanoparticles and nanostructured lipid carriers, further refine release kinetics by enabling biphasic or sustained delivery profiles.[10–14] At the manufacturing level, high-pressure homogenization and ultrasound processing afford precise control over droplet size and spatial distribution within emulsion matrices, directly influencing drug diffusion pathways and release rates.[4] Microneedle co-application strategies are also being actively explored as a means of bypassing the stratum corneum to enhance drug flux from semisolid reservoirs into deeper tissue compartments.[1,7–9]

Essential oils (EOs) have attracted considerable interest as naturally derived antimicrobial agents for incorporation into topical emulsion systems, particularly amid the rise in antibiotic resistance.[15–18] Lavender EO, derived from *Lavandula angustifolia*, is among the most studied, exhibiting broad-spectrum antibacterial activity, primarily attributed to its major constituents, linalool and linalyl acetate, which disrupt microbial membrane integrity and interfere with key metabolic pathways.[19,20] Its favorable safety profile, dermal tolerability, and additional anti-inflammatory properties make it well-suited for topical antimicrobial formulations targeting wound care, burn management, and skin infections.[21,22] The emulsification of EOs presents both an opportunity and a challenge: while it enhances bioavailability and contact with microbial targets through reduced droplet size and increased interfacial area, it requires careful rheological design to ensure physical stability, controlled release, and acceptable application properties.[23–25]

Lactic acid bacteria (LAB) have emerged as an important, if underappreciated, target for topical antimicrobial formulations. Although generally recognized as safe and widely used in food and probiotic products, several LAB strains harbor mobile antibiotic resistance genes (ARGs)—including *tet*(*M*), *tet*(*S*), *erm*(*B*), and *aad*(*E*)—that can be horizontally transferred to pathogenic microorganisms through conjugation and other gene transfer mechanisms.[17,26–30] This capacity to act as reservoirs and vectors of antimicrobial resistance poses significant public health risks, potentially contributing to the spread of resistance through food chains and pharmaceutical

pathways.[29] Effective antimicrobial strategies capable of targeting antibiotic-resistant LAB are therefore of considerable clinical and regulatory interest.

While advanced nanocarriers and stimuli-responsive smart platforms offer undeniable advantages in targeted delivery, a high-molecular-weight (~2 million Da) methyl cellulose (MC) macromolecular matrix was selected for this formulation to meet specific mechanical and practical criteria. MC serves as both a primary thickener and an interfacial stabilizer, completely bypassing the complex, multi-step assembly or high synthetic surfactant loads typical of nanoengineered delivery systems. Furthermore, its network provides an ideal semisolid base with a distinct yield stress (8 Pa) and pronounced shear-thinning behavior, properties essential for uniform patient spreadability and extended physical retention at the topical application site. Most importantly, this classic macromolecular network forms transient polymer entanglements that allow controlled, tunable release via matrix erosion and self-diffusion. This structure can be dynamically altered under mechanical application conditions, providing a practical platform to study how physical agitation accelerates matrix breakdown and enhances EO dispersion. Consequently, this study evaluates the rheological frameworks, transport mechanisms, and accelerated bactericidal kinetics of this formulation, bridging the gap between molecular transport dynamics and practical topical efficacy.

In this study, we developed antibacterial emulsions using triacetin and triethyl citrate as the oil phase and MC as a dual-function thickening and stabilizing agent. No surfactants were utilized. Antibacterial activity was achieved through a synergistic blend of benzyl alcohol, phenylethanol, and lavender EO. The emulsions were comprehensively characterized for their rheological and viscoelastic behavior using Maxwell, Cross, and Herschel–Bulkley modeling frameworks, and *in vitro* EO release studies were conducted under both quiescent and mixed conditions. Antibacterial efficacy was evaluated against *Escherichia coli* and ten genetically diverse LAB strains, with the aim of demonstrating the formulations' potential for both dermatological applications and the control of antibiotic-resistant LAB populations.

2. Materials and methods

2.1. Materials

The MC powder (molecular weight ~2 million Da) was purchased from Fisher Scientific (USA). Triacetin and triethyl citrate (American Chemical Society [ACS] grade) were also obtained from Fisher Scientific. Benzyl alcohol and phenylethanol (ACS grade) were procured from the same supplier. Deionized (DI) water with a resistivity of 18.2 MΩ·cm (Milli-Q® system, MilliporeSigma, USA) was used throughout the study. Steam-distilled lavender oil was sourced from Hiqili Co. (China). N,N-Dimethyl-p-phenylenediamine dihydrochloride (DMPD; 99%) was obtained from Sigma-Aldrich (USA). Povidone-iodine solution (Major Pharmaceuticals, USA) was used to prepare iodinated water for the release studies. Mueller Hinton Broth (Dehydrated) was procured from Thermo Fisher Scientific Inc, USA. Phosphate-buffered saline (PBS) tablets (pH 7.4) were purchased from Sigma-Aldrich (USA). Polysorbate 80 (Tween® 80) and absolute ethanol (99.9% v/v, high-performance liquid chromatography grade) were obtained from Merck KGaA (Germany). Strat-M® synthetic transdermal diffusion membranes (25 mm diameter) were acquired from EMD Millipore (USA).

2.2. Preparation of antibacterial emulsions

The oily phase was prepared by mixing 6 g of triacetin and 6 g of triethyl citrate. Subsequently, 2 g of benzyl alcohol and 2 g of phenylethanol were added to the mixture under shear mixing. While maintaining agitation, 3 g of MC powder was slowly added to the oil phase. This prevented the polymer powder from clumping when water was added. Stirring was continued until the polymer was fully dispersed. Following this, 78 g of DI water was added to the oil-polymer mixture. Emulsification was conducted through two different techniques: shear mixing, where the mixture was treated with a shear mixer (ONILAB OS40 Pro model) at 500 rpm until a white emulsion was produced; and ultrasonic processing, in which emulsification was executed using an ultrasonic processor (US Solid, 20 kHz frequency, 90% amplitude) until a consistent milky texture was attained. Once the emulsion was formed, 1.0 g of lavender oil was added, and the mixing continued for a few additional minutes to ensure homogeneous incorporation of the EO. Table 1 lists three major emulsions we studied, with particular focus on distinguishing and understanding the collective antibacterial efficacy of benzyl alcohol, phenylethanol, and the EO.

As shown in Figure 1A, the shear-mixed emulsion spreads uniformly over the silicone pad surface, indicating good film formation and distribution upon application. Figure 1B highlights the dispersion behavior of the emulsion in the presence of the N,N'-diphenylmethylenediamine-iodine complex. In the left panel of Figure 1B, where the EO-containing emulsion is introduced, the complex solution exhibits a distinct pink to light red coloration. This visual change suggests interaction between the dispersed emulsion and the iodine complex, correlating with ultraviolet–visible light (UV–Vis) spectral modifications at approximately 530 nm, as the emulsion and EO distribute within the aqueous phase.

Conversely, the right panel of Figure 1B shows no clouding when no emulsion is added, confirming the absence of dispersion and interaction under controlled conditions. Further insights are provided in Figure 1C, which shows sequential snapshots of the emulsion's complete miscibility or dispersion in DI water over 8 h. This indicates that the emulsions will uniformly diffuse and disperse in water and other aqueous media, allowing one to measure release rates. Starting from time zero, progressive dispersion is evident at 4 h and 8 h, despite the absence of mechanical stirring. This gradual diffusion behavior may be attributed to spontaneous emulsification driven by interfacial tension gradients and the inherent mobility of dispersed oil droplets within the aqueous phase, as reported in previous studies on emulsifying systems.[31–33]

2.3. Conductivity and rheological characterization

Emulsion conductivity was monitored using a digital benchtop pH-conductivity-total dissolved solid meter (HI 5521, Hanna Instruments, USA). To help identify clear conductivity changes, DI water conductivity was increased by adding sodium chloride salt, and the conductivity was maintained at 400 μS cm^{-1}. Rheological measurements, including viscosity and viscoelastic properties, were conducted using a rheometer (ARES-G2, TA Instruments, USA). To assess the viscoelastic behavior of the emulsions, a plate–plate geometry was used with a 40 mm diameter plate and a 2 mm gap. An oscillatory frequency sweep was performed within the linear viscoelastic region using a constant strain of 0.1%. Measurements were conducted at the equilibrium state of the material to evaluate changes in the elastic storage modulus (G') and viscous loss modulus (G") over a frequency range of 0.1–20 Hz at a controlled temperature of 25.00 ± 0.01 °C. Based on the viscoelastic moduli data, the phase angle (loss tangent), tan δ, defined as the ratio of G" to G', was also calculated to characterize the relative contributions of viscous and elastic behavior.

2.4. Spreadability measurement

Spreadability was determined using the parallel-plate method. A 0.5 g sample of each emulsion was placed on a glass plate, and increasing weights (20–500 g) were applied for 60 s per increment. The spread diameter was measured in two directions using a digital caliper, and the spreadability factor (S) was calculated as $S = (\pi d^2/4) \times (m/t)$, where d is the mean diameter, m is the applied mass, and t is the equilibration time. Measurements were performed in triplicate at 25 ± 0.5 °C, and results are expressed as mean ± standard deviation. Rheological parameters from the rheometer were correlated with spreadability to assess

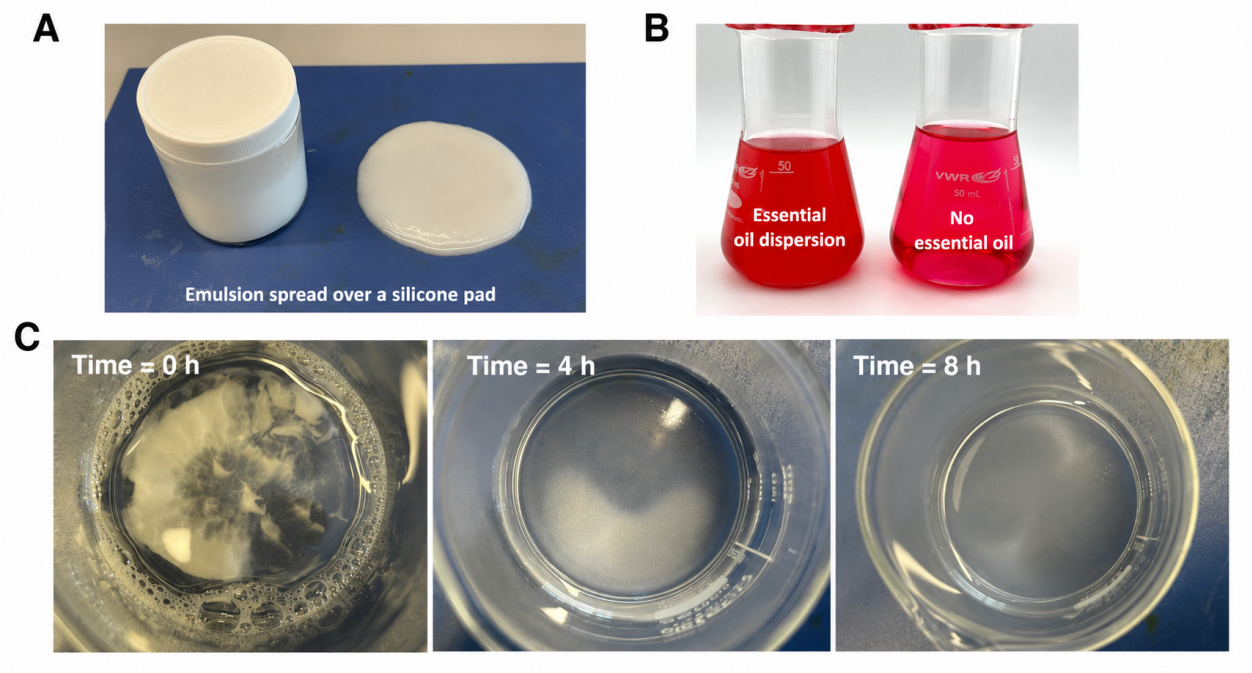


Figure 1. Emulsion spreading, spectroscopic response, and dispersion. (A) Photograph of the emulsion spread over a silicone rubber pad surface. (B) N,N'-diphenylmethylenediamine-iodine complex containing the dispersed emulsion (left beaker) and N,N'-diphenylmethylenediamine-iodine complex in water (right beaker). (C) Top view photograph of 3 g of emulsion dispersing into 100 mL of water over 8 h.

formulation performance.

Table 1. Composition of emulsions (all components in %)

Component	Emulsion 1 (%)	Emulsion 2 (%)	Emulsion 3 (%)
Triethyl citrate	6.0	6.0	6.0
Triacetin	6.0	6.0	6.0
Benzyl alcohol	2.0	0.0	2.0
Phenylethanol	2.0	0.0	2.0
Methyl cellulose	3.0	3.0	3.0
Lavender oil	1.0	1.0	0.0
Deionized water	80.0	84.0	81.0
Total	100.0	100.0	100.0

2.5. Essential oil release measurements

Due to the highly lipophilic and hydrophobic nature of the EO and other additives, a modified receptor medium was used to maintain strict sink conditions throughout the release study. The solubility of the EO was confirmed to be at least three to five times higher in the receptor medium than the maximum predicted concentration at the final sampling interval.

The baseline receptor medium consisted of 0.01 M PBS adjusted to physiological pH 7.40 to simulate biological body fluids. To facilitate wetting and solubilization of the migrated oily phases, the PBS was supplemented with 2.0% (w/v) Polysorbate 80. *In vitro* release kinetics were quantified using a vertical diffusion cell (VDC) test system (Copley HDT 1000, Copley Scientific, UK) equipped with glass VDCs. Each cell possessed a nominal receptor chamber volume of 12.0 mL and an operational diffusion orifice surface area of 1.5 cm^2. A polytetrafluoroethylene (PTFE)-coated magnetic stir bar was placed at the base of each receptor cavity to ensure homogeneous mixing. The jacketed water circulation manifold was linked to a temperature-regulated water bath calibrated to maintain the receptor medium and membrane surface boundary layer at a constant internal physiological body temperature of 37.0 °C. Synthetic Strat-M® membranes were utilized as the rate-limiting barrier to replicate the structural resistance of biological membranes without the inherent biological variability of excised tissues. The membranes were cut to size and pre-conditioned by total immersion in the designated degassed receptor fluid for 30 min to achieve complete hydration.

The receptor cells were filled via their lateral sampling arms with the pre-warmed 37.0 °C receptor medium until a positive meniscus emerged at the orifice rim. The hydrated membrane was carefully positioned horizontally over the upper orifice utilizing flat-tip forceps; a rolling application technique was executed from left to right to purge any residual macro-bubbles from the membrane-fluid interface. The glass donor chamber was aligned directly over the membrane interface and anchored uniformly using a stainless-steel horseshoe clamp mechanism to prevent lateral fluid bypass or volatilization losses. Following assembly, the lateral sampling arm fluid level was adjusted to the designated calibration line, and the system was allowed to equilibrate under continuous magnetic agitation at 300 rpm for 15 min.

At time zero (t = 0), an accurately weighed mass of 300 mg of the emulsion formulation was uniformly applied to the membrane surface in the donor compartment using a positive-displacement micropipette. The donor compartment opening was immediately sealed hermetically using a solvent-resistant high-density polyethylene cap wrapped tightly with laboratory film (Parafilm M®, Amcor, Switzerland). The cells were maintained under constant stirring at 300 rpm. At predetermined time intervals, aliquots of 500 µL were extracted from the geometric center of the receptor chamber through the sampling arm using a long-needle glass syringe. To maintain constant hydrodynamic volume and preserve contact with the membrane underside, an equivalent of fresh, pre-warmed receptor medium was immediately back-filled into the sampling arm. Collected samples were directly transferred into airtight amber glass chromatography vials equipped with PTFE-lined septa and stored at 5 °C.

The release profile of lavender EO from the emulsions was determined spectrophotometrically (Figure 1B) by exploiting the oil's radical-scavenging/antioxidant capacity as a quantitative surrogate marker. Stored samples collected from the receptor chambers were iodinated by adding aliquots of diluted commercial povidone-iodine solution to achieve a final iodine concentration of approximately 60 ppm. Subsequently, 15 mg of DMPD was introduced to the mixture, yielding a characteristic pink-to-red colored radical complex. The presence of the migrated lavender EO altered the intensity of the colored iodine-DMPD complex via concentration-dependent reduction. Control experiments confirmed that the aromatic co-solvents (benzyl alcohol and phenylethanol) exerted negligible independent reduction capacity toward the active iodine-DMPD complex at 530 nm, thereby validating the analytical specificity of the assay for the EO's migrated volatile fraction. The resulting changes in absorbance were monitored using a UV–Vis spectrophotometer at 530 nm, and the cumulative released EO content was quantified using a pre-established calibration curve ($R^2 > 0.99$).

2.6. Bacterial inhibition testing via optical density measurements

The antibacterial efficacy of the formulated emulsions was evaluated by measuring optical density (OD). To fully account for baseline turbidity caused by the progressive spontaneous dispersion of emulsion droplets into the broth, all spectroscopic measurements were blanked against parallel, sterile, cell-free emulsion-broth matrix controls incubated under identical conditions. Two bacterial models were employed: a non-pathogenic strain of *E. coli* (ATCC 10798 [K-12], ATCC, USA) and LAB sourced from a commercial probiotic supplement (Physician's Choice Probiotics 60 Billion Colony-Forming Unit [CFU]-10 Strains), containing a mixture of *Lactobacillus acidophilus* and other LAB species in freeze-dried capsule form. The listing of bacterial species according to the manufacturer is given as *L. acidophilus, Lactobacillus casei, Lactobacillus paracasei, Lactobacillus salivarius, Lactobacillus plantarum, Bifidobacterium lactis, Bifidobacterium bifidum, Bifidobacterium longum, Bifidobacterium breve, Lactobacillus bulgaricus*.

For LAB, freeze-dried powders from the probiotic capsules were rehydrated and activated in de Man, Rogosa, and Sharpe (MRS) broth (Difco Laboratories, USA). The bacterial suspension was incubated at 37 °C for 12–16 h under microaerophilic conditions to allow revival and activation. Following incubation, the culture was diluted in fresh sterile MRS broth to an initial OD_{600} of approximately 0.1 for antibacterial testing. OD measurements were performed in MRS broth to ensure optimal growth conditions throughout the assay. The *E. coli* culture was revived according to ATCC instructions using nutrient broth under aerobic conditions. Prior to testing, both bacterial suspensions were diluted to an initial OD_{600} of approximately 0.1, measured using a UV–Vis spectrophotometer.

Antibacterial testing was conducted by adding approximately 0.5–1.0 g of the prepared emulsions into sterile test tubes containing bacterial suspensions. Control samples without emulsion were prepared in parallel. Tubes were incubated at 37 °C with gentle shaking, and OD_{600} was measured at regular intervals to monitor bacterial growth. Changes in OD values were analyzed as indicators of bacterial inhibition resulting from the release of active compounds from the emulsion formulations. A comparative assessment of treated and control samples was performed to evaluate bacteriostatic or bactericidal effects against both *E. coli* and LAB. OD is a commonly used and convenient method to determine the minimum inhibitory concentration (MIC) of an antimicrobial agent. Although not a direct measure of cell count, OD, typically measured at 600 nm, reflects the solution's turbidity, which is directly related to the biomass of cells present.

2.7. Determination of minimum inhibitory concentration

A pure bacterial culture was prepared and standardized to an OD_{600} of approximately 0.5, equivalent to about 5×10^5 CFU/mL. A series of twofold dilutions of the emulsion was prepared in Mueller–Hinton broth. A standardized suspension of the test organism was added to each dilution, alongside a growth control without antimicrobial agents and a sterile control containing only the medium. The tubes were incubated at 37 °C for 18 h. Post-incubation, OD (turbidity) was measured. The MIC was recorded as the lowest concentration of the antimicrobial agent that prevented visible bacterial growth or an increase in OD relative to the initial inoculum or the sterile control.

2.8. Determination of minimum bactericidal concentration

Following MIC determination, a standard inoculum from each tube or well showing no visible bacterial growth (at or above the MIC) was subcultured onto antibiotic-free agar plates. The plates were incubated at 37 °C for 24 h. The presence or absence of bacterial growth was observed. The minimum bactericidal concentration (MBC) was defined as the lowest concentration of the antimicrobial agent that resulted in a 99.9% reduction (3 $\log_{10}$) in the number of organisms relative to the original inoculum, as indicated by the absence of visible bacterial colonies on the agar plates.

2.9. Modeling viscoelasticity

To characterize the rheological behavior of the MC polymer solution, two well-established empirical-mechanistic models were employed: the generalized Maxwell model for linear viscoelasticity and the Cross model for steady shear viscosity. These models were selected for their ability to capture both frequency-dependent moduli and the shear-thinning behavior observed in semi-dilute MC systems.[34,35] The storage modulus (G') and loss modulus (G") were modeled using a two-mode generalized Maxwell model, which describes the viscoelastic response of materials with discrete relaxation mechanisms. The model equations are shown as **Equations 1 and 2**:

$$G'(\omega) = \sum_{i=1}^{n} \frac{g_i \omega^2 \lambda_i^2}{1 + \omega^2 \lambda_i^2} \quad (1)$$

$$G''(\omega) = \sum_{i=1}^{n} \frac{g_1 \omega \lambda_i}{1 + \omega^2 \lambda_i^2} \quad (2)$$

where g_i is the modulus of the i-th Maxwell element (Pa), λ_i is the corresponding relaxation time (s), ω is the angular frequency (rad/s), and n is the number of Maxwell modes used (here, $n = 2$).

These parameters were tuned to fit the experimental data representing an MC gel with biphasic relaxation dynamics. The two discrete modes capture both fast and slow structural relaxation behavior in the MC network, consistent with literature reports on cellulose derivatives forming transient polymer entanglements.[34,35] To describe the steady shear viscosity behavior, the Cross model was used due to its effectiveness in representing the non-Newtonian flow characteristics of polymer solutions and gels. The model is expressed as **Equation 3**:

$$\eta(\gamma) = \eta_\infty + \frac{\eta_0 - \eta_\infty}{1 + (k_y)^\pi} \quad (3)$$

where $\eta(\gamma)$ is the viscosity at shear rate $\dot{\gamma}$, η_0 is the zero-shear viscosity (Pa·s), η∞ is the infinite-shear viscosity (Pa·s), k is a time constant related to the transition between Newtonian and shear-thinning regimes (s), and m is the power-law index indicating the extent of shear-thinning. This model is particularly suitable for MC systems, which exhibit a broad Newtonian plateau at low shear rates and pronounced shear-thinning due to alignment and disentanglement of the polymer chains at high shear.[36–41]

To investigate the rheological response of the antibacterial emulsion system containing MC, triacetin (6%), triethyl citrate (6%), and a 5% co-solvent blend (benzyl alcohol, phenylethanol, and lavender oil), we employed a Herschel–Bulkley model with thixotropy. This model captures the combined effects of yield stress, shear-thinning, and structural evolution under time-dependent shear. The base flow curve was modeled using the Herschel–Bulkley equation (**Equation 4**):

$$\tau = \tau_y + K\dot{\gamma}^n \quad (4)$$

where τ is the shear stress (Pa), τ_γ is the yield stress (Pa), K is the consistency index (Pa·s^n), n is the flow behavior index (dimensionless), and γ̇ is the applied shear rate (s^{-1}). To incorporate thixotropic behavior, a time-dependent structural parameter λ(t) (ranging from 0 to 1) was introduced, such that (**Equation 5**):

$$\tau = \lambda(t) \cdot \tau_y + K\dot{\gamma}^n \quad (5)$$

The evolution of λ(t) was governed by the kinetic **Equation 6**:

$$\frac{d\lambda}{dt} = k_{\text{build}}(1-\lambda) - k_{\text{break}}\lambda|\dot{\gamma}| \quad (6)$$

where $k_{rebuild}$ is the structural recovery rate (s^{-1}), and k_{break} is the rate of structural breakdown due to shear (s^{-1}). The viscosity η was computed from the ratio $\eta = \tau/\dot{\gamma}$. This model was selected because it accurately represents the yield stress and hysteresis behavior commonly observed in emulsified and gelled systems stabilized by amphiphilic plasticizers and aromatic co-solvents.[39–41] The model effectively describes the yielding transition, which is a hallmark of semi-solid emulsions, where flow only occurs beyond a critical stress threshold; viscosity hysteresis, which is characteristic of time-dependent breakdown and rebuild of gel structures; and nonlinear flow behavior important for predicting real-world application performance, including extrudability, spreadability, and retention on the skin. Model parameters were selected based on typical values for thixotropic gels (τ_γ = 8 Pa, K = 15 Pa·s^n, n = 0.65), and simulations were conducted over a shear rate range of 0.1 to 100 s^{-1} for both increasing and decreasing ramps.

2.10. Drug release kinetic models

Drug release from the emulsions was tested in two different conditions. The first was self-diffusion of the emulsion (Figure 1C), and the second was shear mixing. Several widely accepted drug release kinetic models were also evaluated. The Weibull model, an empirical model suitable for various release kinetics, is defined as **Equation 7**:

$$F(t) = 1 - e^{-\left(\frac{t}{\tau}\right)^\beta} \quad (7)$$

where $F(t)$ is the fraction of drug released at time t, τ is the scale parameter (indicating time to 63.2% release), and β is the shape factor.[16] The Korsmeyer–Peppas model is commonly used for polymeric matrix systems (**Equation 8**):

$$F(t) = kt^n \quad (8)$$

where k is a kinetic constant, and n is the release exponent that indicates the mechanism of release.[15] The Higuchi model assumes a diffusion-controlled process based on Fick's law (**Equation 9**):

$$F(t) = k_H t^{1/2} \quad (9)$$

where k_H is the Higuchi constant, representing the rate of drug release.[12] The First-order model is described by a concentration-dependent release rate (**Equation 10**):

$$\frac{dF}{dt} = k\left(1 - F\right) \tag{10}$$

Solving **Equation 10** yields **Equation 11**:

$$F(t) = 1 - e^{-kt} \tag{11}$$

where k is the first-order release constant.[14] The performance of each model was evaluated using R^2, root mean square error (RMSE), and Akaike information criterion (AIC) values, and the results were tabulated.

3. Results and discussion

3.1. Conductivity changes during emulsification

Figure 2 shows the temporal conductivity profiles of oil-in-water emulsions prepared using mechanical mixing and high-shear homogenization. Both correspond to Emulsion 1 in Table 1. The progressive decrease in conductivity reflects the continuous dispersion of non-conductive oil droplets into the conductive aqueous phase. As emulsification progresses, the conductive continuous phase becomes increasingly obstructed by dispersed oil droplets, thereby reducing ion mobility and measurable conductivity.[40,41]

Both datasets were modeled using an exponential decay combined with a linear recovery component to capture the kinetics of droplet dispersion and subsequent stabilization effects (**Equation 12**):

$$y(t) = A \cdot e^{-Bt} + C \cdot t + D \tag{12}$$

where A and B describe the amplitude and rate of conductivity loss due to droplet formation, while C and D account for slower phase interactions and the final plateau conductivity, respectively.

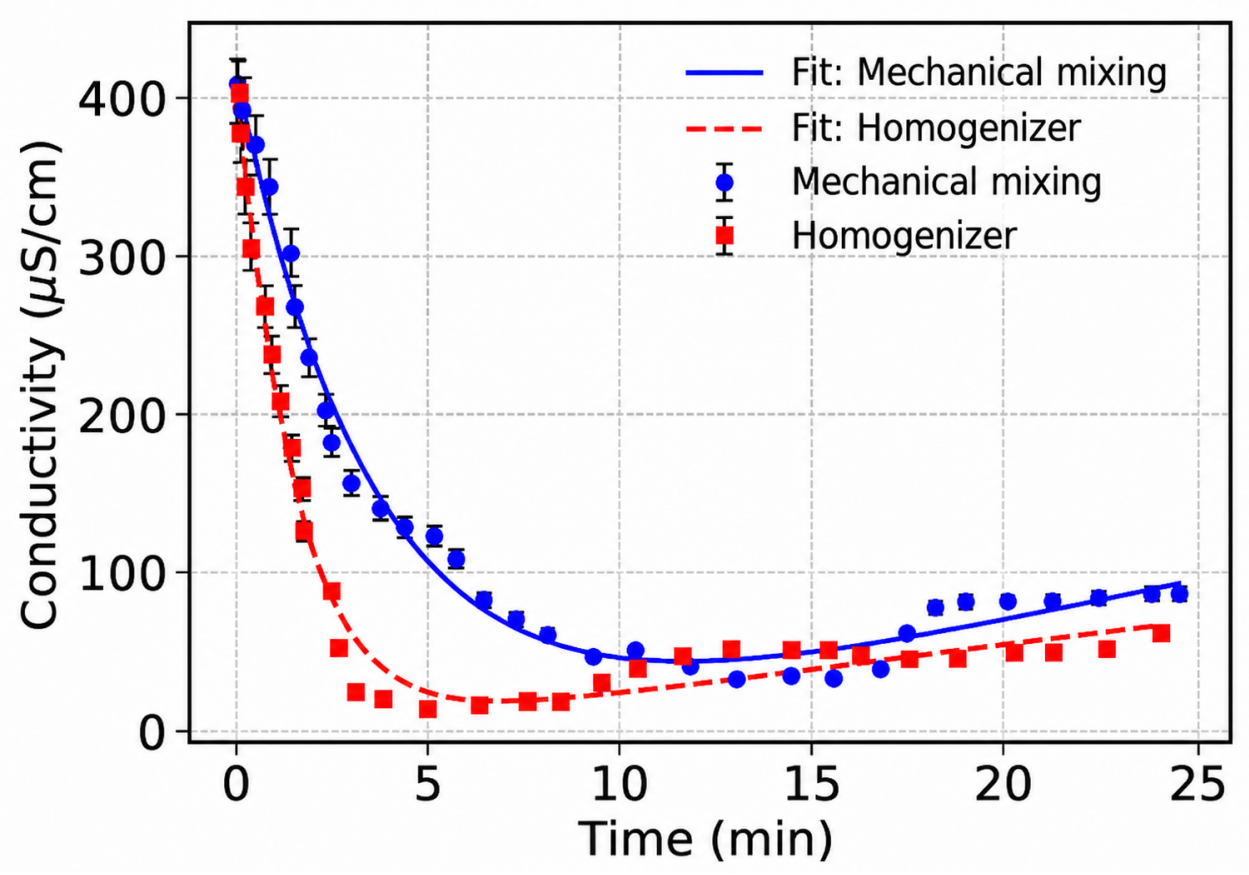


Figure 2. Comparison of conductivity changes over time for mechanical mixing and homogenizer treatments during emulsification. Fits are based on exponential decay plus linear recovery. Error bars represent the range of uncertainty in data collection.

3.2. Effect of mixing method

Homogenizer-treated emulsion exhibited a much sharper and more immediate decline in conductivity, consistent with the high shear and cavitation forces generated during homogenization. As detailed in a previous study, such forces enable efficient droplet breakup by overcoming interfacial tension more effectively than mechanical mixing.[41] This results in the rapid creation of fine, uniformly dispersed oil droplets that quickly block ionic pathways in the continuous phase. Mechanical mixing, by contrast, produced a more gradual decline in conductivity, indicating slower emulsification kinetics and less efficient droplet dispersion. The relatively lower energy input in mechanical mixing limits the ability to disrupt and disperse oil phases, leading to larger droplets and delayed conductivity reduction.

Interestingly, the mechanical mixing process showed a minor recovery in conductivity over longer timescales. This could indicate droplet recoalescence or structural reorganization, possibly due to insufficient energy input to maintain stable small droplets. This behavior aligns with the weaker dispersion stability observed in lower-shear systems, as highlighted in prior emulsification studies.[39–41] Homogenization produced emulsions with lower plateau conductivity and more stable droplet distributions, as confirmed by lower D values and higher decay rates (B) from the fitted models. This reflects the formation of smaller, more stable droplets that are resistant to coalescence, which are critical for producing long-term, stable emulsions. In contrast, mechanical mixing, while less effective in reducing conductivity rapidly, may be preferred in formulations where excessive shear could compromise sensitive components, such as the breakdown of bulky polymeric ingredients.[40]

3.3. Interpretation of fitted parameters

The fitted model parameters presented in Table 2 provide insights into the emulsification kinetics and the structural evolution of oil-in-water emulsions produced using mechanical mixing and homogenization.

Table 2. Fitted model parameters for conductivity reduction during oil-in-water emulsification using mechanical mixing and homogenization

Parameter	Unit	Mechanical mixing	Homogenizer
A	μS/cm	450.95	419.87
B	hr^{-1}	0.2707	0.6539
C	μS/(cm·hr)	5.2438	3.0758
D	μS/cm	−36.26	−6.65

The amplitude parameter A, representing the magnitude of the initial conductivity drop, was higher for the mechanically mixed samples (450.95 μS/cm) than for the homogenized emulsions (419.87 μS/cm). This suggests that the mechanically mixed system retained higher initial ionic conductivity, likely because non-conductive oil droplets dispersed more slowly in the early stages of emulsification. The decay rate constant B was notably higher for the homogenizer samples (0.6539 hr^{-1}) compared to mechanical mixing (0.2707 hr^{-1}). This indicates that homogenization facilitated faster emulsification, as the high shear and cavitation effects rapidly dispersed the oil phase and reduced the continuous phase's conductivity. The recovery slope C was larger in the mechanically mixed system (5.2438 μS/(cm·hr)) than in the homogenized samples (3.0758 μS/(cm·hr)). This suggests that the mechanical mixing process enabled slow structural rearrangements or partial recoalescence over time, contributing to a gradual increase in conductivity as ionic pathways were partially restored.

Finally, the plateau offset parameter D was negative for both processes but less negative for the homogenized emulsions (−6.65 μS/cm) compared to mechanical mixing (−36.26 μS/cm). This negative offset is likely a mathematical artifact of the exponential decay plus linear recovery model, representing an overshoot effect beyond the physical conductivity minimum. Nonetheless, the lower negative D value in homogenizer-treated samples further supports the formation of a more stable and homogeneously dispersed emulsion, with a reduced likelihood of structural recoalescence. Overall, these parameters quantitatively confirm that homogenization promotes faster, more stable emulsification relative to mechanical mixing, consistent with the observed conductivity trends.[39,41] Using conductivity as a surrogate marker for droplet dispersion provides a novel, indirect yet practical approach to track emulsion formation and stabilization. However, care must be exercised during ultrasonic processing of polymeric emulsions as molecular weights can be modified during this process.[41]

3.4. Viscoelasticity of methyl cellulose solutions

Figure 3A illustrates the frequency-dependent viscoelastic response of a 3 wt.% MC solution in water characterized by the storage modulus (G') and loss modulus (G") modeled using a two-element Maxwell model. The data align well with the expected behavior of structured semi-solid systems, where G' dominates at higher frequencies, indicating elastic-dominant behavior, while G" prevails at lower frequencies, reflecting viscous contributions. This dual behavior is typical of pharmaceutical emulsions and gels, in which microstructural elements, such as

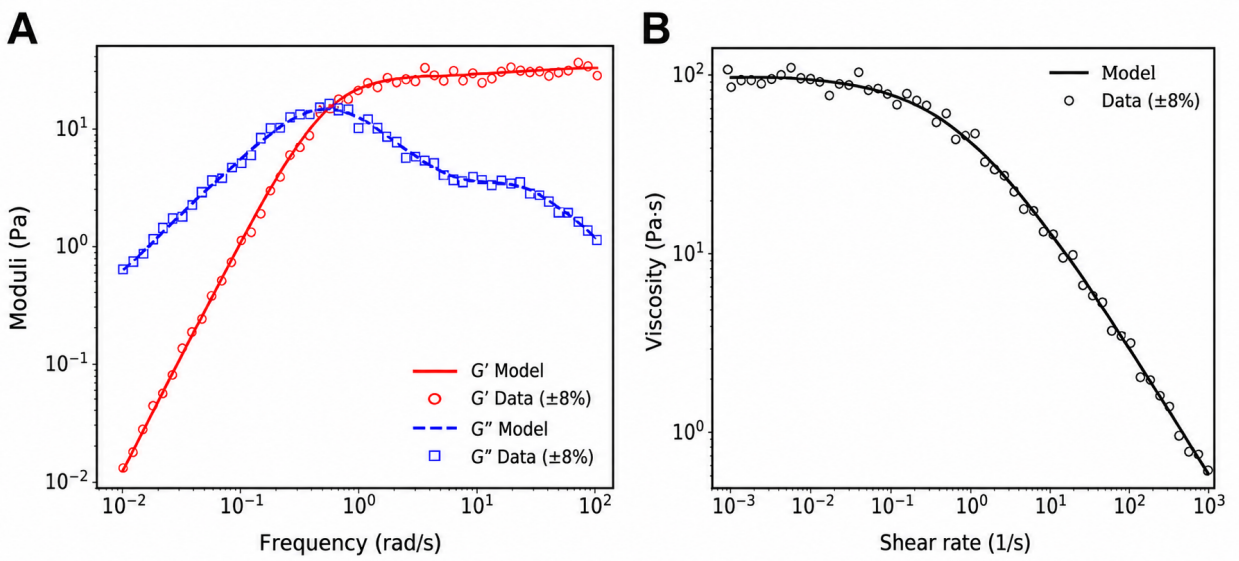


Figure 3. Three percent methyl cellulose solution in water. (A) Frequency-dependent storage modulus (G') and loss modulus (G") fitted using a two-element Maxwell model. (B) Shear-rate dependent viscosity modeled using the Cross model. In both panels, open symbols represent experimental data.

droplet interfaces or polymer networks, contribute to viscoelasticity.[31–34] The scatter in the experimental data captures the variability commonly observed in experimental rheometry, especially in formulations that undergo interfacial or hydration dynamics over time.[2,34] The sharp crossover behavior between G' and G" supports the assumption of a dominant relaxation mode, which is often used in simplified modeling of topical delivery systems.[6,35]

3.5. Shear-thinning

Figure 3B shows the shear rate-dependent viscosity modeled using the Cross model. This empirical model effectively captures the shear-thinning behavior typical of semi-solid formulations such as emulgels, nanoemulsions, and lipid-based gels.[42,43] The viscosity decreases by several orders of magnitude with increasing shear rate, which facilitates spreadability and patient compliance upon topical application.[9,10] The high zero-shear viscosity (η_0 ~ 100 Pa·s) and the low infinite-shear viscosity ($\eta\infty$ ~ 0.001 Pa·s) suggest the formulation has strong internal network structures at rest that break down under mechanical stress. This characteristic is advantageous for controlled drug release as it ensures structural integrity during storage and flowability during application.[3,7]

3.6. Implications for topical drug delivery systems

Understanding the viscoelastic and flow properties of pharmaceutical emulsions is critical for optimizing drug release kinetics and enhancing dermal penetration. Systems exhibiting high elasticity at relevant physiological frequencies can maintain longer residence times on the skin and resist deformation, thus modulating release.[2,14] Moreover, formulations with pronounced shear-thinning allow for improved application characteristics, reduced dosing variability, and better spreadability on curved or irregular skin surfaces.[1,8] The combination of Maxwell and Cross modeling, as demonstrated in Figure 3, offers a predictive framework to rationally design semi-solid systems that meet the dual requirements of mechanical stability and patient usability. Future work may incorporate temperature dependence and thixotropic recovery to better simulate *in vivo* application conditions.[11]

3.7. Viscoelasticity of the antibacterial emulsions

Figure 4 presents the rheological characterization of the antibacterial emulsion system containing triacetin, triethyl citrate, aromatic alcohols, and the EO (Emulsion 1). The data are shown for both upward and downward shear rate ramps to highlight hysteresis effects in flow and viscosity behavior.

The rheological behavior was modeled using a Herschel–Bulkley constitutive equation augmented with a thixotropic structural parameter λ(t) to capture the time-dependent microstructural changes under shear. This parameter evolves according to competing breakdown and rebuild kinetics described in **Equation 6**, where k_{break} and $k_{rebuild}$ govern the rates of structural degradation and recovery, respectively.

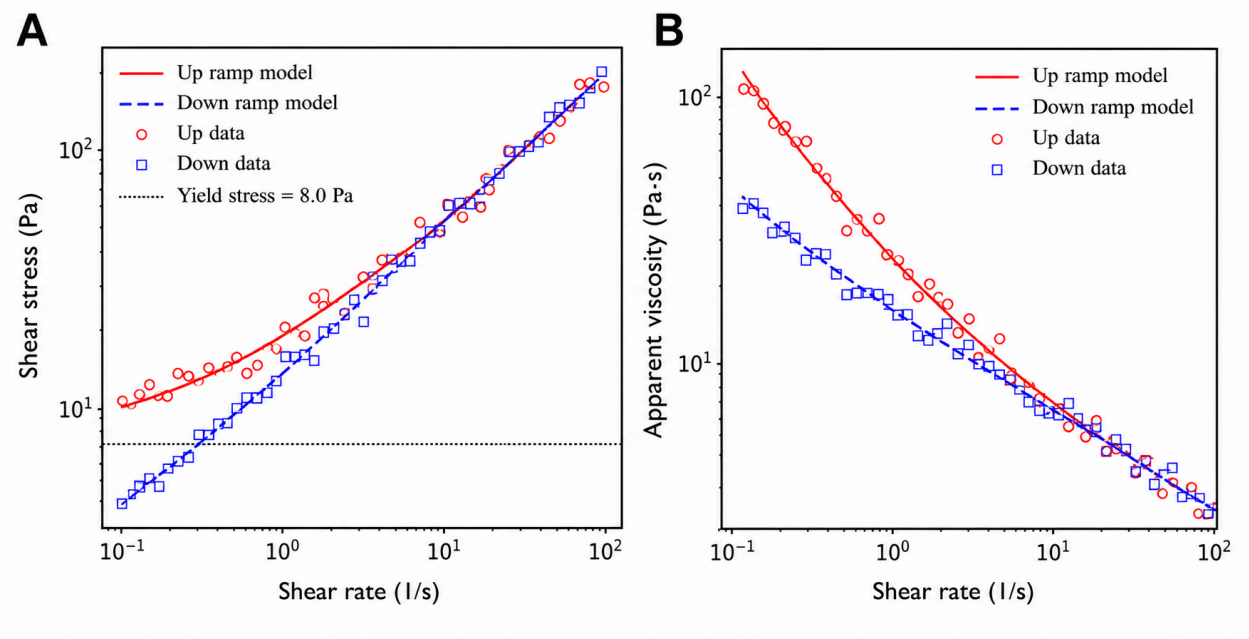


Figure 4. Rheological properties of the antibacterial emulsion system, Emulsion 1. (A) Flow curves displaying shear stress as a function of shear rate for increasing (solid red) and decreasing (dashed blue) ramps, including experimental data. The yield stress, indicated by the horizontal dotted line, demonstrates the critical stress threshold required for flow initiation. (B) Apparent viscosity hysteresis loops showing viscosity versus shear rate during the upward and downward ramps, illustrating the time-dependent breakdown and recovery of the material's internal structure.

As seen in Figure 4A, the upward shear rate ramp exhibits a pronounced yield stress behavior, with shear stress remaining near the yield value τ_y = 8 Pa until flow initiates. The downward ramp deviates from the upward curve, indicating hysteresis due to the formulation's thixotropic nature. This behavior reflects the breakdown of the internal gel-like network upon shearing and its partial recovery during relaxation.[33,34] Figure 4B further emphasizes this hysteresis via viscosity measurements. The apparent viscosity decreases sharply as shear rate increases during the upward ramp, demonstrating shear-thinning. Upon decreasing shear rate, the viscosity follows a different path, forming a loop that confirms the material's time-dependent structural evolution. The model's inclusion of $\lambda(t)$ successfully captures these complex dynamics and aligns well with the experimental data.

The choice of the Herschel–Bulkley plus thixotropy model is appropriate for this emulsion system due to its ability to represent the yield stress character typical of semi-solid emulsions and polymer gels[33,34]; non-Newtonian shear-thinning flow behavior arising from polymer chain disentanglement and emulsifier action[3,35]; and time-dependent structural breakdown and rebuilding under cyclic shear, crucial for predicting application performance such as spreadability and stability.[40,41] Incorporation of plasticizers (triacetin, triethyl citrate) and aromatic co-solvents (benzyl alcohol, phenylethanol, lavender oil) modifies the microstructure and interfacial properties of the MC network, affecting the parameters controlling thixotropic behavior.[37–43] The antimicrobial properties of these additives additionally contribute to formulation stability.[44–47] Overall, the good agreement between model predictions and experimental data validates the model's utility for describing and optimizing antibacterial topical emulsion formulations.

In Figure 5, the shear-mixed formulation exhibited consistently higher spreadability compared to the no-shear formulation across all applied masses. At an applied mass of 100 g, the shear-mixed emulsion achieved a mean spread diameter of 35.1 ± 0.6 mm, corresponding to a spreadability factor of 1,613 mm²·g/s, whereas the no-shear formulation reached only 30.8 ± 0.7 mm (S = 1,242 mm²·g/s)—representing a 30% increase attributable to shear processing. The spreadability ratio (final diameter / initial diameter) was 3.43 for the shear-mixed formulation.

Power-law fits to the data revealed exponents of 0.71 (shear-mixed) and 0.73 (no-shear), confirming the shear-thinning nature of both formulations. The measured yield stress of 8 Pa, determined from rheometric measurements, correlates with the initial resistance to spreading observed at low applied masses. These spreadability values are within the range reported for other semisolid topical formulations

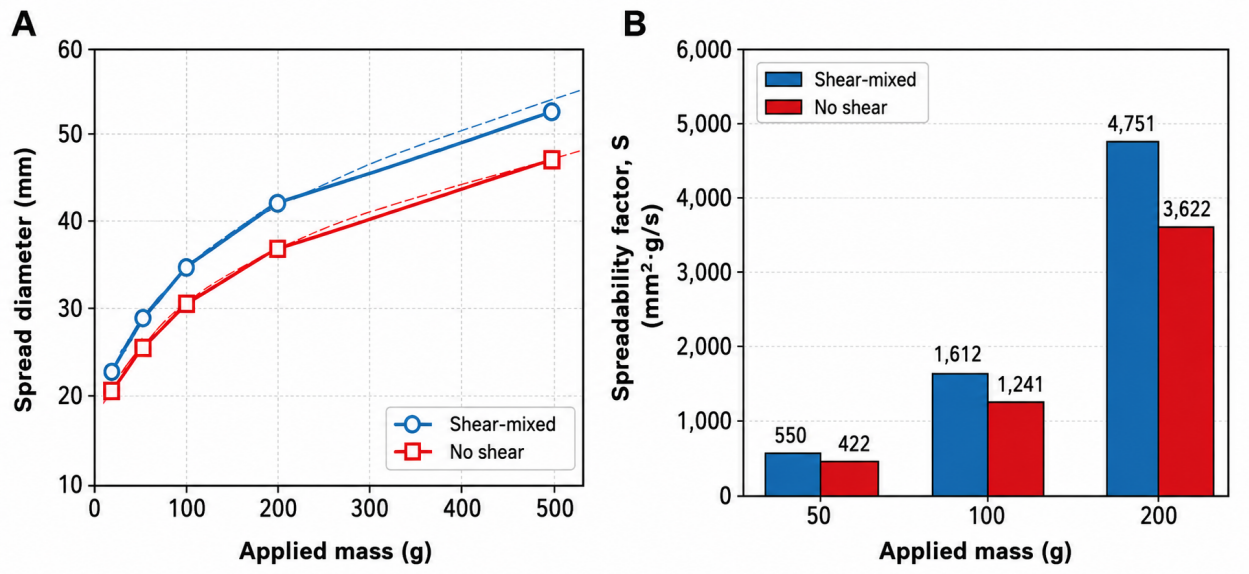


Figure 5. Spreadability of Emulsion 1 evaluated using the parallel-plate method. (A) Spread diameter as a function of applied mass for shear-mixed (circles) and no-shear (squares) formulations. Error bars represent standard deviation (n = 3). Dashed lines represent power-law fits. The yield stress of 8 Pa is annotated. (B) Spreadability factor (S) at selected applied masses (50, 100, and 200 g), showing the enhancement attributable to shear processing.

(S = 900–1,800 mm²·g/s)[41–43], confirming that Emulsion 1 possesses acceptable application characteristics. The enhanced spreadability of the shear-mixed formulation is attributed to microstructural disruption and reduced polymer chain entanglement, consistent with the rheological data presented in this section.

3.8. Drug release analysis

Lavender EO, derived from *L. angustifolia*, has demonstrated notable antibacterial activity against a broad spectrum of Gram-positive and Gram-negative bacteria due to its high content of linalool and linalyl acetate, which disrupt microbial membranes and metabolic pathways.[18,19] These properties have made lavender oil an attractive component in pharmaceutical emulsions, where it serves as both an active antimicrobial agent and a fragrance enhancer.[21] In emulsified formulations, lavender oil can enhance stability by participating in the oil phase and may contribute synergistically when combined with preservatives like benzyl alcohol or phenylethanol.[46] Moreover, its natural origin and minimal toxicity make it favorable for dermatological applications, particularly in formulations aimed at treating wounds, burns, and skin infections.[47,48]

The drug release kinetics were analyzed for both the original emulsion and gently mixed systems, with fitting results presented separately in Table 3 (original) and Table 4 (mixed). The comparative release profiles are shown in Figure 6.

Table 3. Model fitting results for the original emulsion system

Model	Parameters	R^2	RMSE (%)	AIC
Weibull	τ = 5.24, β = 2.59	0.985	4.56	112.3
Korsmeyer–Peppas	k = 6.05, n = 0.75	0.963	6.82	125.7
Higuchi	k_H = 29.12	0.932	8.91	138.2
First-order	k = 0.42	0.876	11.34	152.9

Abbreviations: AIC: Akaike information criterion; RMSE: Root mean square error.

Table 4. Model fitting results for the gently mixed system

Model	Parameters	R^2	RMSE (%)	AIC
Weibull	τ = 1.21, β = 1.45	0.997	1.52	89.5
Korsmeyer–Peppas	k = 35.20, n = 0.63	0.993	2.89	98.3
Higuchi	k_H = 42.85	0.962	5.12	115.6
First-order	k = 0.57	0.945	6.24	122.8

Abbreviations: AIC: Akaike information criterion; RMSE: Root mean square error.

The Weibull model demonstrated superior performance for both systems, achieving the highest R^2 values (0.985 for original, 0.997 for mixed) and lowest AIC scores (112.3 and 89.5, respectively) as shown in Tables 3 and 4. This model's accuracy is further supported by the low RMSE values (4.56% for the original and 1.52% for the mixed), which were 3–4 times lower than those of alternative models. The shear-mixed system showed consistently better fit quality across all metrics, suggesting more

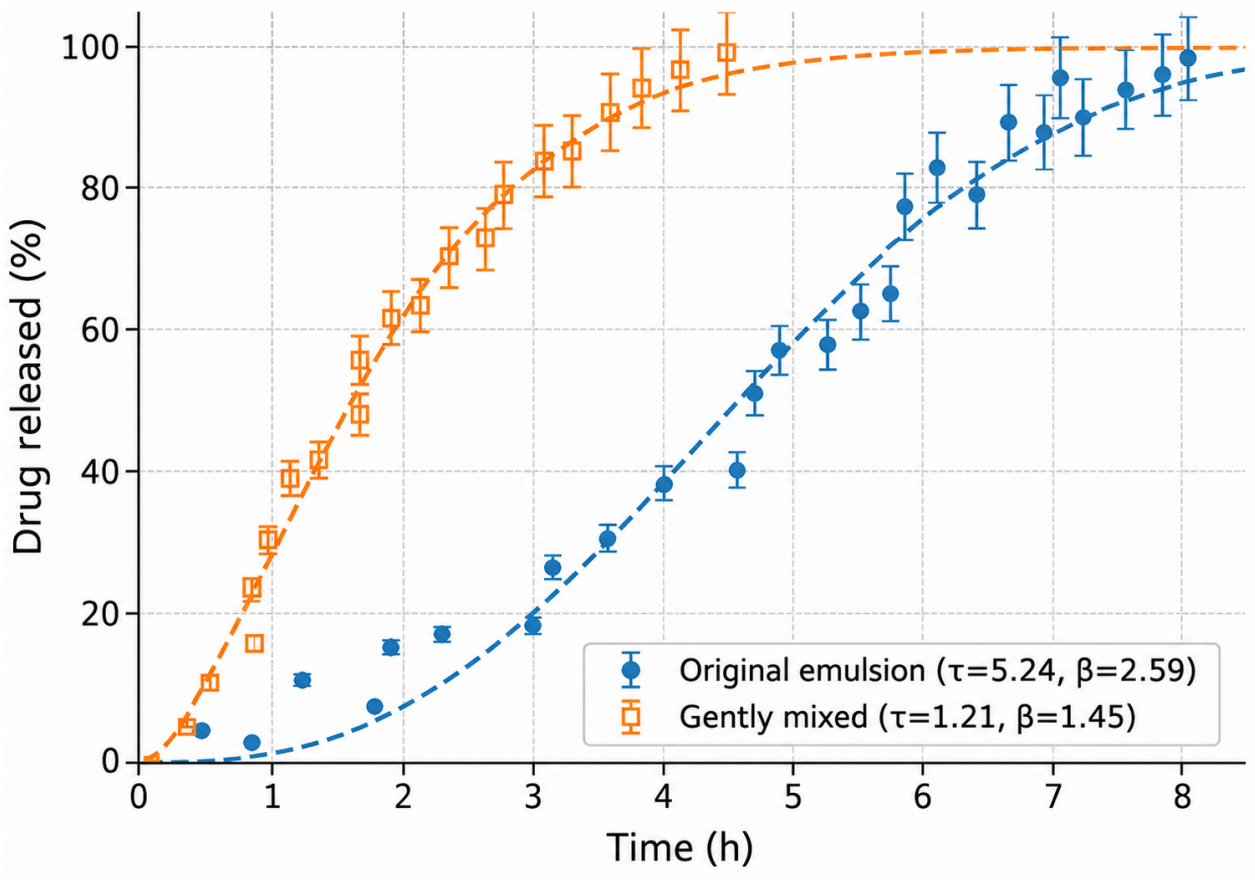


Figure 6. Drug release profiles comparing original emulsion (blue circles, solid fit line) and gently mixed system (orange squares, dashed fit line). Error bars represent the uncertainty range in measurements.

predictable release kinetics. Comparative analysis of the Weibull parameters reveals significant differences between systems. The original emulsion exhibited a longer timescale (τ = 5.24 h) and more pronounced sigmoidal character (β = 2.59), indicating gradual matrix hydration followed by accelerated release. In contrast, the gently mixed system showed faster release (τ = 1.21 h) with reduced sigmoidicity (β = 1.45), suggesting immediate drug accessibility due to microstructural disruption. These kinetic differences are visually apparent in Figure 6, where the mixed system's profile lacks the distinct lag phase seen in the original emulsion. The decline in sigmoidicity from 2.59 to 1.45 is a clear indication of changes in the release mechanism, likely related to disruption of polymer entanglements and matrix erosion.

The scatter in measured data in Figure 6 demonstrates good experimental reproducibility across all time points. The tighter error margins for the mixed system (Table 4, RMSE = 1.52%) compared to the original emulsion (RMSE = 4.56%) may reflect greater homogeneity induced by mixing. The Korsmeyer–Peppas model also provided excellent fits (R^2 > 0.99) for both systems, with release exponent n values (0.63–0.75) confirming anomalous transport mechanisms combining diffusion and erosion. The high β value (> 2) for the original emulsion indicates strong sigmoidal behavior, characteristic of systems with initial lag phases followed by accelerated release. This pattern reflects gradual matrix hydration and subsequent erosion-dominated drug liberation, consistent with previous reports.[14,49–52] In contrast, the reduced β in the mixed system suggests more immediate drug accessibility, likely due to mixing-induced disruption of the emulsion microstructure.

3.9. Growth inhibition and bactericidal activity

The MIC and MBC results presented in Table 5 indicate a clear enhancement of antibacterial efficacy when benzyl alcohol and phenylethanol are incorporated into the non-aqueous phase of the emulsions. Against both *E. coli* and LAB strains, emulsions containing 2% benzyl alcohol and 2% phenylethanol exhibited significantly lower MIC

and MBC values compared to formulations lacking these additives. Specifically, for *E. coli*, the MIC decreased from 0.60% to 0.35%, and the MBC from 1.00% to 0.85% upon inclusion of the aromatic alcohols. A similar trend was observed for LAB, with the MIC reducing from 0.75% to 0.55% and the MBC from 1.50% to 0.95%. These findings suggest that benzyl alcohol and phenylethanol act synergistically with the EO components to enhance membrane disruption and permeabilization, thereby enhancing bacterial inhibition and bactericidal activity. Both compounds are small aromatic alcohols with known antimicrobial properties and the capacity to disrupt lipid bilayers, facilitating penetration of active compounds into bacterial cells.[46,47,53] Their amphiphilic character likely assists in destabilizing microbial membranes, thus enhancing the activity of the dispersed EO phase.

Moreover, the observed reduction in both MIC and MBC values across Gram-negative (*E. coli*) and Gram-positive (LAB) bacteria underscores the broad-spectrum potential of these additives when incorporated into antibacterial emulsion systems. While the emulsions without benzyl alcohol and phenylethanol still exhibited antimicrobial activity, the increased MIC and MBC values confirm the role of these compounds as potentiators rather than primary antimicrobials. In summary, the inclusion of benzyl alcohol and phenylethanol enhances both dispersion efficacy and antimicrobial activity of the emulsified EO system, offering a promising formulation strategy for broad-spectrum antibacterial applications.

3.10. Modeling microbial population data

Figure 7 illustrates the OD decay over time for different emulsions subjected to antibacterial treatment, including two control emulsions and cases with no mixing and shear mixing. The OD values can be indirectly correlated to bacterial concentration, with reduction indicating bactericidal activity. To model the bacterial reduction data, a generalized logistic decay model was employed, defined as **Equation 13**:

$$N(t) = N_{\infty} + \frac{N_0 - N_{\infty}}{1 + (k \times t)^{\beta}} \quad (13)$$

where N(t) represents the bacterial concentration (in $\log_{10}$ CFU/mL) at time t, N_0 is the initial bacterial load, N_{∞} is the lower asymptote (final bacterial load), k is the decay rate, and β is a shape parameter controlling the steepness of the decline. This model was chosen for its ability to capture the nonlinear dynamics of bacterial inactivation, including initial lag phases, rapid declines, and asymptotic behavior, which are common in microbial reduction studies.[54–56]

The logistic model offers several advantages over simpler models, such as linear or power-law decay functions. Unlike the power-law model, which assumes a fixed initial value and lacks a lower asymptote, the logistic model allows for a variable initial bacterial load (N_0) and a final plateau (N_{∞}), accommodating datasets with diverse starting points and saturation effects.[56] This flexibility is particularly relevant for the four datasets analyzed: Control 1 (no antibacterials), Control 2 (benzyl alcohol + phenylethanol, no EO), no mixing, and gently mixing. For instance, Control 1 exhibits minimal reduction, remaining near 9 $\log_{10}$ CFU/mL, while gently mixing (500 rpm shear rotation) shows a rapid decline followed by a plateau near 3 $\log_{10}$ CFU/mL.

The model was fitted to each dataset using nonlinear least-squares regression, implemented via the curve_fit function in SciPy.[57] Initial parameter guesses were set as N_0 = 9.0, N_{∞} = 2.0, k = 0.5, and β = 1.0, based on the observed data ranges. The fits successfully captured the distinct behaviors of the datasets: Control 1's near-constant profile, Control 2's gradual decline, and the sharper reductions in no mixing and gently mixing cases. The model's logistic form effectively described the asymptotic behavior in Control 2 and gently mixing, where bacterial counts stabilized, and its shape parameter (β) adjusted the transition steepness, particularly for the rapid decline in gently mixing. Error bars and the fitted curves generally fell within these uncertainties, indicating robust fits. Figure 7 illustrates the experimental data and fitted curves for all four datasets.

The generalized logistic model aligns with established microbial inactivation frameworks, such as those described by Geeraerd *et al.*[55], which emphasize the need

Table 5. Minimum inhibitory concentration (MIC) and minimum bactericidal concentration (MBC) of emulsions containing different non-aqueous phase ingredients against *E. coli* and lactic acid bacteria (LAB)

Bacteria	Triethyl citrate (%)	Triacetin (%)	Benzyl alcohol (%)	Phenylethanol (%)	MIC (%)	MBC (%)
E. coli	6.0	6.0	2.0	2.0	0.35	0.85
E. coli	6.0	6.0	0.0	0.0	0.60	1.00
LAB	6.0	6.0	2.0	2.0	0.55	0.95
LAB	6.0	6.0	0.0	0.0	0.75	1.50

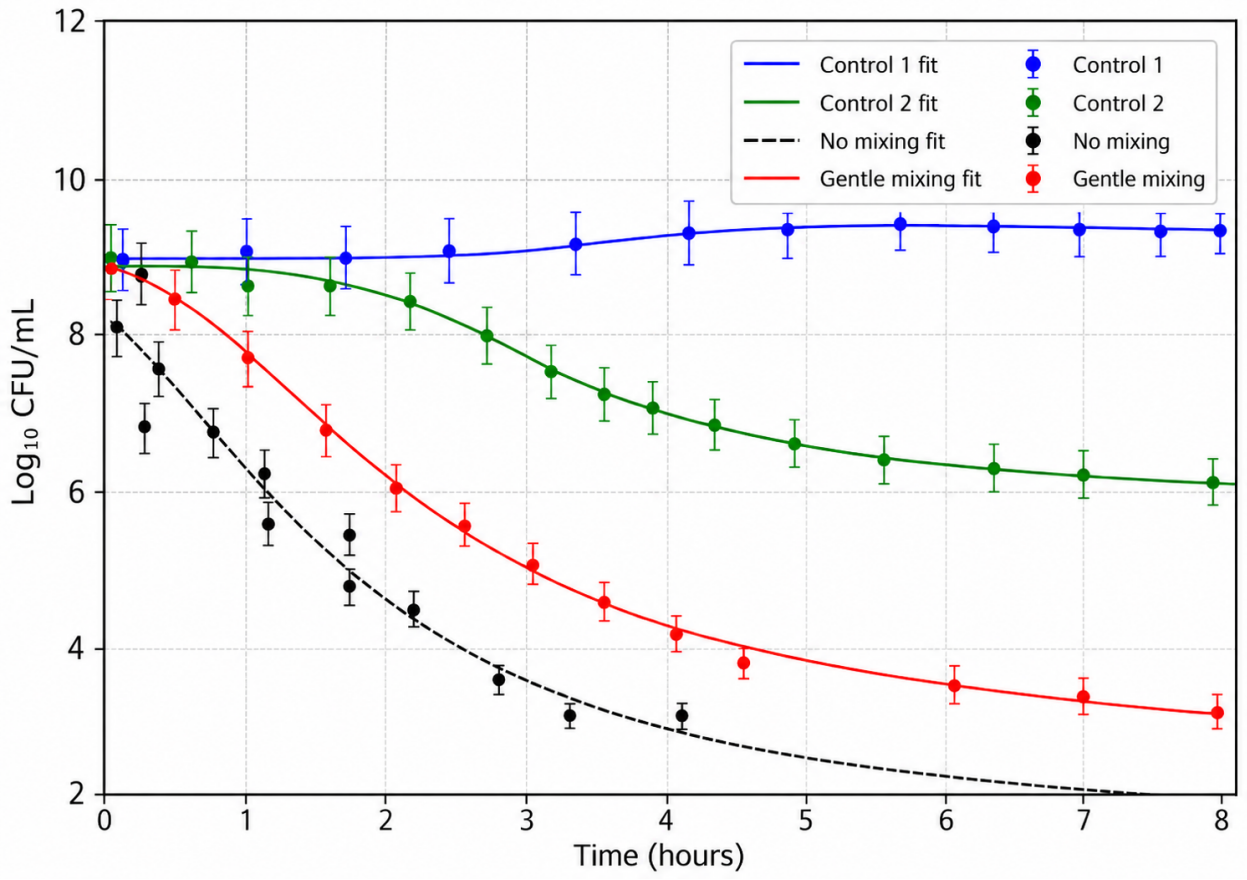


Figure 7. Bacterial reduction data and fitted generalized logistic decay curves for four datasets: Control 1 (no antibacterials, blue circles), Control 2 (benzyl alcohol + phenylethanol, no essential oil, green circles), no mixing (black circles), and gently mixing (red circles). Mixing cases are done with Emulsion 1. Solid and dashed lines represent the fitted models, with error bars. Gently mixing here refers to shear mixing at 500 rpm.
Abbreviation: CFU: Colony-forming unit.

for models that account for lag phases and tailing effects. Its application here ensures biologically meaningful parameters and improved fit quality compared to the power-law models, particularly for datasets with minimal reduction or plateauing behavior.[56] Control emulsions exhibit minimal to moderate reduction over 8 h, indicative of stable bacterial populations or natural die-off. In contrast, the shear mixing case shows significantly accelerated bactericidal activity, reflected in a higher rate constant k and a β parameter suggesting a complex time dependence, possibly due to enhanced antibacterial agent distribution or increased shear stress.[54] The no mixing case shows intermediate behavior, with slower reduction than the mixed sample, underscoring the role of physical agitation in antimicrobial efficacy. These findings align with prior studies demonstrating that mixing can improve contact between antimicrobials and bacteria, thereby enhancing bactericidal activity.[58]

3.11. Bactericidal effects on lactic acid bacteria

Several strains of LAB exhibit varying degrees of antibiotic resistance, both phenotypically and genotypically, and may serve as reservoirs of transferable resistance determinants.[15–18,58] Common resistance traits include resistance to aminoglycosides, vancomycin, and quinolones, while acquired genes such as *tet*(*M*), *tet*(*S*), *erm*(*B*), and *aad*(*E*) have been reported in food- and probiotic-associated LAB.[15–18,58] Horizontal transfer of antibiotic-resistance genes among LAB has also been demonstrated experimentally, highlighting their potential role in dissemination of antimicrobial resistance through food and clinical ecosystems.[18] Considering that LAB can act as vectors for antibiotic resistance—particularly when they harbor mobile ARGs—it is critical to assess the antimicrobial performance of novel formulations. We monitored changes in OD_{600} over time to evaluate the efficacy of our antibacterial emulsions against LAB, as the EO was dispersed into the bacteria-laden medium. As

illustrated in Figure 8, four conditions were tested: Control 1 (no antibacterial agent), Control 2 (benzyl alcohol + phenylethanol), Emulsion 1 without mixing, and Emulsion 1 with mixing.

In Control 1, LAB exhibited continual growth, as evidenced by the rising OD_{600} values over 8 h. As such, no decay model could be fitted. Control 2, which showed a modest inhibitory effect from benzyl alcohol and phenylethanol, did not prevent growth, indicating that these alcohols alone have limited antimicrobial activity. However, both emulsion formulations containing lavender EO demonstrated significant inhibitory effects, consistent with documented antimicrobial properties of lavender EO against various microorganisms, including LAB, *E. coli*, multidrug-resistant *Staphylococcus aureus*, and vancomycin-resistant *Enterococcus*.[20,58] In particular, the no-mixing lavender oil formulation induced a gradual decrease in OD, indicating slower release and diffusion of the antimicrobial EO. In contrast, the mixed formulation produced a rapid, steep decline in OD, implying enhanced dispersion, smaller droplet size, and faster release kinetics, thereby amplifying antibacterial efficacy. This observation aligns with prior studies showing that nano- and microemulsions of EOs exhibit superior antimicrobial effects due to increased surface area and membrane disruption.[43,44,53]

Quantitatively, the mixed lavender formulation achieved an approximate 60–70% reduction in OD within the first 3 h, compared to about 30–40% reduction in the no-mix formulation over the same period. These results underscore the importance of formulation method in maximizing antibacterial performance.[59] Overall, our findings suggest that mechanical mixing significantly improves EO dispersion and antimicrobial efficacy,

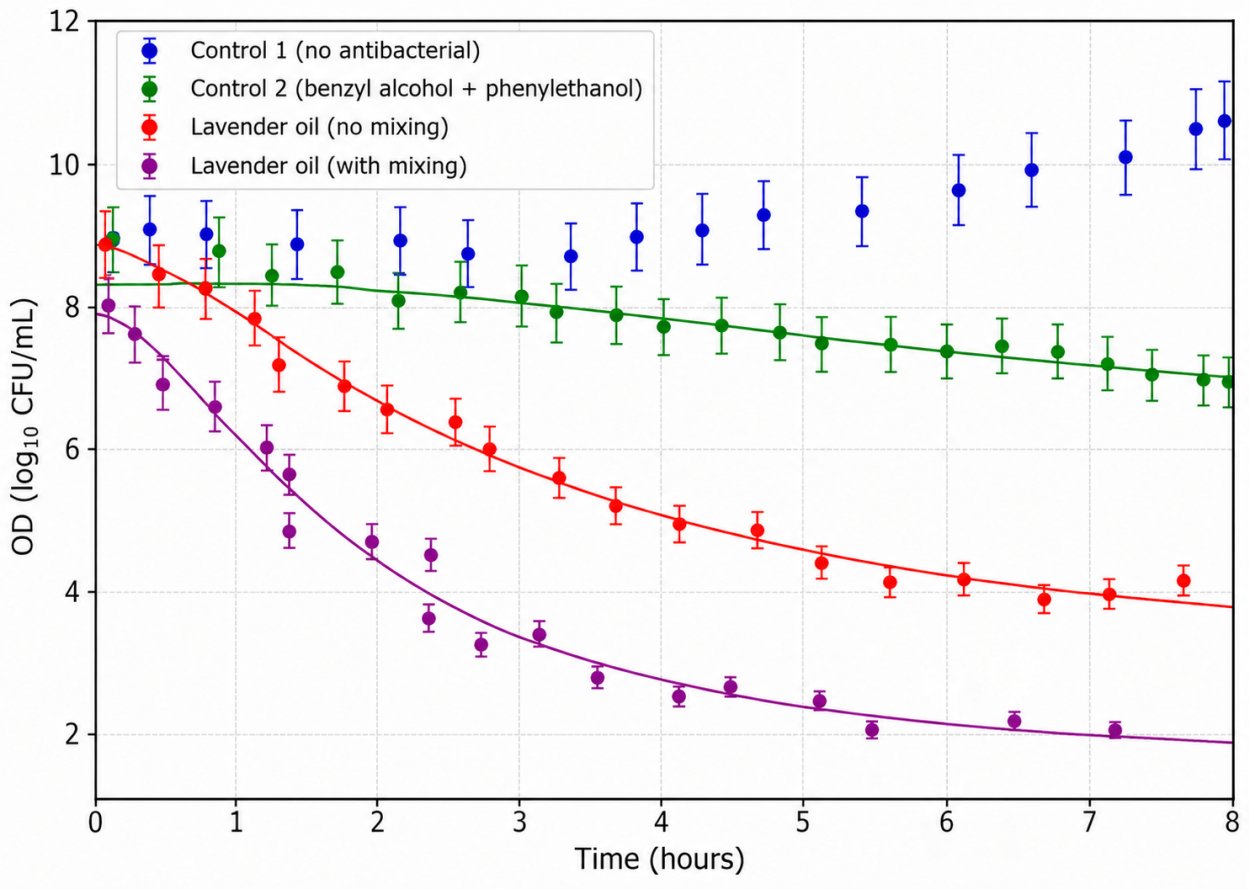


Figure 8. Optical density (OD) profiles of lactic acid bacteria cultures over time under four different treatment conditions: (i) Control 1: Bacteria in nutrient medium without any antibacterial agent (blue markers), (ii) Control 2: Bacteria exposed to benzyl alcohol and phenylethanol emulsion without essential oil (green markers), (iii) Lavender oil emulsion prepared without mechanical mixing (red markers), and (iv) Lavender oil emulsion prepared with high-shear mixing (magenta markers). Error bars represent variability based on replicate measurements. Solid lines indicate the logistic decay model fits to the experimental data.

Abbreviations: CFU: Colony-forming unit; OD: Optical density.

transforming a bacteriostatic effect into a rapid bactericidal response against *LAB*. The reduction of OD—an indicator of cell death or growth arrest—supports the potential application of such antibacterial emulsions for controlling antibiotic-resistant *LAB* carriers in both clinical and food-chain contexts. The antibacterial potency of lavender EO against Gram-positive and Gram-negative bacteria is well documented. MICs typically range between 0.625 and 35.0 mg/mL for *E. coli* and *S. aureus*.[58] This may be approximately translated into 0.06% to 3.5%. Emulsification enhances this effect, as shown in studies in which EO microemulsions inhibited bacterial growth at concentrations as low as 0.8%.[23,24,59] Our findings align with these results, showing that the mixed formulation exerts potent antimicrobial activity at comparable EO levels. By focusing on *LAB* as vectors of ARGs, our study highlights a novel application niche for such EO emulsions—namely, preventing the spread of resistance genes—beyond the typical scope of food preservation or surface disinfection. Further work should include viability assays (e.g., CFU counts) and membrane-interaction studies to comprehensively validate these formulations for applied use. In summary, the following observations have been evident:

(i) Microstructure ↔ antimicrobial activity: The processing condition that produced faster droplet dispersion (steeper conductivity decay) also produced faster oil release (Weibull $\tau = 1.21$ vs 5.24 h) and faster bactericidal activity. We interpret these as a single underlying cause: finer, more uniformly dispersed droplets present a larger oil–water interfacial area, increasing the rate at which membrane-active constituents (linalool, linalyl acetate, benzyl alcohol, phenylethanol) reach and disrupt the bacterial membrane.

(ii) Rheology ↔ skin retention: The measured yield stress (8 Pa) together with shear-thinning and thixotropic recovery describes a material that flows under the shear of application but rebuilds structure at rest—the rheological basis for spreadability during application and residence on the skin afterward.

(iii) Release ↔ bactericidal activity: We now place the Weibull release profiles alongside the logistic bactericidal activity curves and note that both accelerate together under mixing. This is consistent with a release-limited (rather than composition-limited) bactericidal action: the rate at which the active fraction becomes available, not merely its total amount, governs the bactericidal activity—directly supporting the central thesis of the paper.

4. Conclusion

This study demonstrates that antibacterial emulsions based on MC and lavender EO can be rationally engineered to achieve tunable rheological behavior and enhanced antimicrobial performance through deliberate formulation design. The emulsions exhibited well-characterized viscoelastic properties—including a yield stress of 8 Pa, pronounced shear-thinning, and thixotropic recovery—that are desirable for topical applications requiring spreadability, skin retention, and structural stability during storage. The Herschel–Bulkley model with a structural parameter $\lambda(t)$ provided an accurate mechanistic description of these behaviors, offering a practical predictive tool for future formulation optimization. Table 6 shows the similarities or differences between the emulsions formulated in this work and those available in the literature.

The EO release kinetics were decisively influenced by processing method: shear (gentle) mixing reduced

Table 6. The present formulation compared to the closest prior art that uses the triacetin/triethyl citrate emulsion platform

Ester/stabilizer platform	Reported application	Distinction from this work	Reference
Triacetin + medium-chain triacylglycerols as the oil–water oil phase; surfactant-stabilized	Chemical stabilization of citral flavor in beverage emulsions	Food/flavor; no antibacterial function, methyl-cellulose gel, or processing–bactericidal activity analysis	60
Triacetin/triethyl citrate dispersing medium + methyl cellulose viscosifier + polysorbate	Storage-stable citrus-flavor encapsulation (liquid water enhancers)	Flavor encapsulation in a non-aqueous medium; no antibacterial actives, release/bactericidal activity, or resistance-vector target	61
Triacetin-mixed oil–water emulsion; emulsifier + mono-/polyhydric alcohols	Fine, highly stable oil-soluble-component emulsions	Food emulsion; no aromatic-alcohol/EO antibacterial system or rheology–bactericidal activity modeling	62
Methyl cellulose + triacetin/ triethyl citrate + benzyl alcohol/ phenylethanol + lavender EO	Topical antibacterial emulsion vs. *E. coli* and resistant lactic acid bacteria	Antibacterial application; processing-as-determinant; conductivity & DMPD–iodine assays; ARG-vector targeting	This study

Abbreviations: ARG: Antibiotic resistance gene; DMPD: N,N-Dimethyl-p-phenylenediamine dihydrochloride; EO: Essential oil.

the Weibull time parameter τ from 5.24 h to 1.21 h and suppressed the lag phase associated with matrix hydration, consistent with microstructural disruption and increased interfacial area. The superior fit of the Weibull model across both conditions (R^2 = 0.985 and 0.997) underscores its suitability for characterizing release from complex emulsified matrices.

The inclusion of benzyl alcohol and phenylethanol produced synergistic reductions in MIC and MBC against both *E. coli* and LAB—with MBC values dropping by 15–37%—confirming that aromatic alcohols serve as potentiators rather than primary antimicrobials. Critically, the mixed emulsion formulation transformed a bacteriostatic response into a rapid bactericidal response, achieving 60–70% reduction in OD_{600} within 3 h against LAB strains known to carry horizontally transferable ARGs. This finding positions the formulation strategy not only as a dermatological tool but also as a potential intervention to limit the spread of antimicrobial resistance via LAB vectors in the food chain and clinical settings.

Taken together, these results establish a clear principle: formulation method—particularly mixing intensity—is as consequential as chemical composition in determining both physical and antimicrobial performance. Future work should include *in vivo* skin penetration studies, accelerated-stability testing, CFU-based viability assays, and membrane-interaction studies to advance these emulsions toward applied use.

Acknowledgments

None.

Funding

This study is supported by Gempa Electromechanical Engineering Ltd. Co.

Conflict of interest

Gözde Bayer is an employee of Gempa Electromechanical Engineering Ltd. Co., which provided funding for this study. The remaining authors declare no competing interests.

Author contributions

Conceptualization: Ilker S. Bayer
Data curation: All authors
Investigation: Gozde Bayer, Amirreza Shayganpour
Methodology: Gozde Bayer, Amirreza Shayganpour
Supervision: Ilker S. Bayer
Writing–original draft: Ilker S. Bayer
Writing–review and editing: Ilker S. Bayer
All authors have read and agreed to the published version of the manuscript.

Ethics approval and consent to participate

Not applicable.

Consent for publication

Not applicable.

Availability of data

Data are available from the corresponding author upon reasonable request.

Further disclosure

The original, non-peer-reviewed manuscript has been uploaded onto Preprints.org (doi: 10.20944/preprints202507.2466.v1).

References

1. Qu F, Geng R, Liu Y, Zhu J. Advanced nanocarrier- and microneedle-based transdermal drug delivery strategies for skin diseases treatment. *Theranostics*. 2022;12(7):3372-3406.
   doi: 10.7150/thno.69999
2. Yukuyama MN, Kato ET, Lobenberg R, Bou-Chacra N. Challenges and future prospects of nanoemulsion as a drug delivery system. *Curr Pharm Des*. 2017;23(3):495-508.
   doi: 10.2174/1381612822666161027111957
3. Charman SA, Charman WN, Rogge MC, Wilson DT, Dutko FJ, Pouton CW. Self-emulsifying drug delivery systems: formulation and biopharmaceutic evaluation of an investigational lipophilic compound. *Pharm Res*. 1992;9(1):87-93.
   doi: 10.1023/A:1018987928936
4. Rodriguez J, Martín MJ, Ruiz MJG, Clares B. Current encapsulation strategies for bioactive oils: from alimentary to pharmaceutical perspectives. *Food Res Int*. 2016;83:41-59.
   doi: 10.1016/j.foodres.2016.01.032
5. Stefanov SR, Andonova VY. Lipid nanoparticulate drug delivery systems: recent advances in the treatment of skin disorders. *Pharmaceuticals*. 2021;14(11):1083.
   doi: 10.3390/ph14111083
6. Jeong WY, Kwon M, Choi HE, Kim KS. Recent advances in transdermal drug delivery systems: a review. *Biomater Res*. 2021;25(1):24.
   doi: 10.1186/s40824-021-00226-6
7. Raina N, Rani R, Thakur VK, Gupta M. New insights in topical drug delivery for skin disorders: from a nanotechnological perspective. *ACS Omega*. 2023;8(22):19145-19167.

doi: 10.1021/acsomega.2c08016

8. Opatha SAT, Titapiwatanakun V, Chutoprapat R. Transfersomes: a promising nanoencapsulation technique for transdermal drug delivery. *Pharmaceutics*. 2020;12(9):855.

doi: 10.3390/pharmaceutics12090855

9. Tran M, Wang C. Semi-solid materials for controlled release drug formulation: current status and future prospects. *Front Chem Sci Eng*. 2014;8(2):225-232.

doi: 10.1007/s11705-014-1429-7

10. Zhang H, Pan Y, Hou Y, Li M, Deng J, Wang B, Hao S. Smart physical-based transdermal drug delivery system: towards intelligence and controlled release. *Small*. 2024;20(9):e2306944.

doi: 10.1002/smll.202306944

11. Bushi E, Malaj L, Di Martino P, Mataj G, Myftari B. Formulation of semi solid dosage forms for topical application utilizing quality by design (QbD) approach. *Drug Dev Ind Pharm*. 2025;51(7):670-678.

doi: 10.1080/03639045.2025.2498521

12. Papadopoulou V, Kosmidis K, Vlachou M, Macheras P. On the use of the Weibull function for the discernment of drug release mechanisms. *Int J Pharm*. 2006;309(1-2):44-50.

doi: 10.1016/j.ijpharm.2005.10.044

13. Kosmidis K, Argyrakis P, Macheras P. A reappraisal of drug release laws using Monte Carlo simulations: the prevalence of the Weibull function. *Pharm Res*. 2003;20(7):988-995.

doi: 10.1023/A:1024497920145

14. Corsaro C, Neri G, Mezzasalma MAM, Fazio E. Weibull modeling of controlled drug release from Ag-PMA nanosystems. *Polymers*. 2021;13(17):2897.

doi: 10.3390/polym13172897

15. Chaves CRS, Salamandane A, Vieira EJF, Salamandane C. Antibiotic resistance in fermented foods chain: evaluating the risks of emergence of enterococci as an emerging pathogen in raw milk cheese. *Int J Microbiol*. 2024;2024(1):2409270.

doi: 10.1155/ijm/2409270

16. Nawaz M, Wang J, Zhou A, Ma C, Ma C, Wu X, Moore J, Millar BC, Xu J. Characterization and transfer of antibiotic resistance in lactic acid bacteria from fermented food products. *Curr Microbiol*. 2011;62(3):1081-1089.

doi: 10.1007/s00284-010-9856-2

17. Floris I, Battistini R, Tramuta C, Garcia-Vozmediano A, Musolino N, Scardino G, Masotti C, Brusa B, Orusa R, Serracca L, et al. Antibiotic resistance in lactic acid bacteria from dairy products in Northern Italy. *Antibiotics*. 2025;14(4):375.

doi: 10.3390/antibiotics14040375

18. Jian Z, Zeng L, Xu T, Sun S, Yan S, Yang L, Huang Y, Jia J, Dou T. Antibiotic resistance genes in bacteria: occurrence, spread, and control. *J Basic Microbiol*. 2021;61(12):1049-1070.

doi: 10.1002/jobm.202100201

19. Anisimova E, Yarullina D. Antibiotic resistance of *Lactobacillus* strains. *Curr Microbiol*. 2019;76(12):1407-1416.

doi: 10.1007/s00284-019-01769-7

20. Yusupova U, Tojiboeva D, Mukhamatkhanova R, Dusmatova D. Essential oils as an alternative to synthetic antiseptics in cosmetics and personal care products. *Chem Biodivers*. 2026;23(1):e03449.

doi: 10.1002/cbdv.202503449

21. Wells R, Truong F, Adal AM, Sarker LS, Mahmoud SS. *Lavandula* essential oils: a current review of applications in medicinal, food, and cosmetic industries of lavender. *Nat Prod Commun*. 2018;13(10).

doi: 10.1177/1934578X1801301038

22. Samuelson R, Lobl M, Higgins S, Clarey D, Wysong A. The effects of lavender essential oil on wound healing: a review of the current evidence. *J Altern Complement Med*. 2020;26(8):680-690.

doi: 10.1089/acm.2019.0286

23. Zuzarte M, Gonçalves M, Cavaleiro C, Canhoto J, Vale-Silva L, Silva M, Pinto E, Salgueiro L. Chemical composition and antifungal activity of the essential oils of *Lavandula viridis* from Portugal. *J Med Microbiol*. 2011;60(5):612-618.

doi: 10.1099/jmm.0.027748-0

24. Garcia CR, Malik MH, Biswas S, Tam VH, Rumbaugh KP, Li W, Liu X. Nanoemulsion delivery systems for enhanced efficacy of antimicrobials and essential oils. *Biomater Sci*. 2022;10(3):633-653.

doi: 10.1039/D1BM01537K

25. Bakkali F, Averbeck S, Averbeck D, Idaomar M. Biological effects of essential oils: a review. *Food Chem Toxicol*. 2008;46(2):446-475.

doi: 10.1016/j.fct.2007.09.106

26. Nunziata L, Brasca M, Morandi S, Silvetti T. Antibiotic resistance in wild and commercial non-enterococcal lactic acid bacteria and bifidobacteria strains of dairy origin: an update. *Food Microbiol*. 2022;104:103999.

doi: 10.1016/j.fm.2022.103999

27. Botina SG, Poluektova E, Glazova A, Zakharevich NV, Koroban N, Zinchenko V, Babykin M, Zhilenkova O, Amerkhanova A, et al. Antibiotic resistance of potential probiotic bacteria of the genus *Lactobacillus* from human gastrointestinal microbiome. *Microbiology*. 2011;80(2):164-171.

doi: 10.1134/S0026261711020032

28. Toomey N, Monaghan A, Fanning S, Bolton D. Transfer of antibiotic resistance marker genes between lactic acid bacteria in model rumen and plant environments. *Appl Environ Microbiol*. 2009;75(10):3146-3152.

doi: 10.1128/AEM.02471-08

29. Gad GF, Abdel-Hamid AM, Farag ZS. Antibiotic resistance in lactic acid bacteria isolated from some pharmaceutical and dairy products. *Braz J Microbiol*. 2014;45(1):25-33.

doi: 10.1590/S1517-83822014000100005

30. Samtiya M, Matthews KR, Dhewa T, Puniya AK. Antimicrobial resistance in the food chain: trends, mechanisms, pathways, and possible regulation strategies. *Foods*. 2022;11(19):2966.

doi: 10.3390/foods11192966

31. Tadros TF. Emulsion formation, stability, and rheology. In: *Emulsion Formation and Stability*. Wiley; 2013:1-75.

doi: 10.1002/9783527647941.ch1

32. Wu X, Xue H, Bordia G, Fink Z, Kim PY, Streubel R, Han J, Helms BA, Ashby PD, Omar AK, Russell TP. Self-propulsion by directed explosive emulsification. *Adv Mater*. 2024;36(19):2310435.

doi: 10.1002/adma.202310435

33. Forgiarini A, Esquena J, González C, Solans C. Formation of nano-emulsions by low-energy emulsification methods at constant temperature. *Langmuir*. 2001;17(7):2076-2083.

doi: 10.1021/LA001362N

34. Dabbaghi M, Namjoshi S, Panchal B, Grice J, Prakash S, Roberts M, Mohammed YH. Viscoelastic and deformation characteristics of structurally different commercial topical systems. *Pharmaceutics*. 2021;13(9):1351.

doi: 10.3390/pharmaceutics13091351

35. Herbig ME, Evers DH, Gorissen S, Köllmer M. Rational design of topical semi-solid dosage forms—how far are we? *Pharmaceutics*. 2023;15(7):1822.

doi: 10.3390/pharmaceutics15071822

36. Salim N, Ahmad N, Musa SH, Hashim R, Tadros TF, Basri M. Nanoemulsion as a topical delivery system of antipsoriatic drugs. *RSC Adv*. 2016;6(8):6234-6250.

doi: 10.1039/C5RA14946K

37. McClements DJ. *Food Emulsions: Principles, Practices, and Techniques*. 2nd ed. CRC Press; 2004.

doi: 10.1201/9781420039436

38. Walstra P. *Physical Chemistry of Foods*. CRC Press; 2001.

doi: 10.1201/9780203910436

39. Karasulu HY. Microemulsions as novel drug carriers: the formation, stability, applications and toxicity. *Expert Opin Drug Deliv*. 2008;5(1):119-135.

doi: 10.1517/17425247.5.1.119

40. Villay A, De Filippis F, Picton L, Cerf D, Vial C, Michaud P. Comparison of polysaccharide degradations by dynamic high-pressure homogenization. *Food Hydrocoll*. 2012;27(2):278-286.

doi: 10.1016/J.FOODHYD.2011.10.003

41. Qayum A, Rashid A, Liang Q, Wu Y, Cheng Y, Kang L, Liu Y, Zhou C, Hussain M, Ren X, et al. Ultrasonic and homogenization: an overview of the preparation of an edible protein–polysaccharide complex emulsion. *Compr Rev Food Sci Food Saf*. 2023;22(6):4242-4281.

doi: 10.1111/1541-4337.13221

42. Kumbhar P, Desai H, Desai V, Priya S, Rana V, Singhvi G. Versatility of emulgel in topical drug delivery: transforming its expedition from bench to bedside. *Expert Opin Drug Deliv*. 2025;22(1):55-68.

doi: 10.1080/17425247.2024.2439457

43. Ojha B, Jain VK, Gupta S, Talegaonkar S, Jain K. Nanoemulgel: a promising novel formulation for treatment of skin ailments. *Polym Bull*. 2021;79(7):4441-4465.

doi: 10.1007/s00289-021-03729-3

44. Ciocarlan A, Lupascu L, Aricu A, Dragalin I, Popescu V, Geană E, Ionete R, Vornicu N, Duliu O, Hristozova G, et al. Chemical composition and assessment of antimicrobial activity of lavender essential oil and some by-products. *Plants*. 2021;10(9):1829.

doi: 10.3390/plants10091829

45. Manjanna KM, Gouda BV, Tanusha AS, Ankita S, Anusha H, Arpita J. Formulation and evaluation of capsaicin transemulgel for the treatment of arthritis. *J Drug Deliv Ther*. 2025;15(1):73-83.

doi: 10.22270/jddt.v15i1.6946

46. Bayer IS. Fungal quorum sensing molecules as potential drugs in the treatment of chronic wounds and their delivery. *Expert Opin Drug Deliv*. 2025;22(2):277-296.

doi: 10.1080/17425247.2025.2452303

47. Sulaiman M , Hassan Y, Tok T, Noundou X. Synthesis, antibacterial activity and docking studies of benzyl alcohol derivatives. *J Turk Chem Soc Sect A Chem*. 2020;7(2):481-488.

doi: 10.18596/jotcsa.692113

48. Singh Y, Meher J, Raval K, Khan FA, Chaurasia M, Jain N, Chourasia MK. Nanoemulsion: concepts, development and applications in drug delivery. *J Control Release*. 2017;252:28-49.

doi: 10.1016/j.jconrel.2017.03.008

49. Askarizadeh M, Esfandiari N, Honarvar B, Sajadian SA,

Azdarpour A. Kinetic modeling to explain the release of medicine from drug delivery systems. *ChemBioEng Rev*. 2023;10(6):1006-1049.

doi: 10.1002/cben.202300027

50. Moser K, Kriwet K, Naik A, Kalia YN, Guy RH. Passive skin penetration enhancement and its quantification in vitro. *Eur J Pharm Biopharm*. 2001;52(2):103-112.

doi: 10.1016/S0939-6411(01)00166-7

51. Setti C, Suarato G, Perotto G, Athanassiou A, Bayer IS. Investigation of in vitro hydrophilic and hydrophobic dual drug release from polymeric films produced by sodium alginate–MaterBi drying emulsions. *Eur J Pharm Biopharm*. 2018;130:71-82.

doi: 10.1016/j.ejpb.2018.06.019

52. Ignacio M, Chubynsky MV, Slater GW. Interpreting the Weibull fitting parameters for diffusion-controlled release data. *Physica A*. 2017;486:486-496.

doi: 10.1016/j.physa.2017.05.033

53. Cavanagh H, Wilkinson J. Biological activities of lavender essential oil. *Phytother Res*. 2002;16(4):301-308.

doi: 10.1002/ptr.1103

54. Peleg M. *Advanced Quantitative Microbiology for Foods and Biosystems: Models for Predicting Growth and Inactivation*. CRC Press; 2006.

doi: 10.1201/9781420005370

55. Geeraerd AH, Valdramidis VP, Van Impe JF. GInaFiT, a freeware tool to assess non-log-linear microbial survivor curves. *Int J Food Microbiol*. 2005;102(1):95-105.

doi: 10.1016/j.ijfoodmicro.2004.11.038

56. Whiting RC. Microbial modeling in foods. *Crit Rev Food Sci Nutr*. 1995;35(6):467-494.

doi: 10.1080/10408399509527711

57. Virtanen P, Gommers R, Oliphant TE, Haberland M, Reddy T, Cournapeau D, Burovski E, Peterson P, Weckesser W, Bright J, et al. SciPy 1.0: fundamental algorithms for scientific computing in Python. *Nat Methods*. 2020;17(3):261-272.

doi: 10.1038/s41592-019-0686-2

58. Wax RG, Lewis K, Salyers AA, Taber H. *Bacterial Resistance to Antimicrobials*. 2nd ed. CRC Press; 2007.

doi: 10.1201/9781420008753

59. Mouton JW, Vinks AA. Pharmacokinetic/pharmacodynamic modelling of antibacterials in vitro and in vivo using bacterial growth and kill kinetics. *Clin Pharmacokinet*. 2005;44(2):201-210.

doi: 10.2165/00003088-200544020-00005

60. Choi SJ, Decker EA, Henson L, Popplewell LM, McClements DJ. Stability of citral in oil-in-water emulsions prepared with medium-chain triacylglycerols and triacetin. *J Agric Food Chem*. 2009;57(23):11349-11353.

doi: 10.1021/jf902761h

61. Givaudan SA. Flavour composition. Patent WO2015185553A1. Published December 10, 2015. https://patents.google.com/patent/WO2015185553A1/en

62. T Hasegawa Co Ltd. Triacetin-mixed oil-in-water type emulsion composition. Patent JP2011045316A. Published March 10, 2011. https://patents.google.com/patent/JP2011045316A/en